JMB

Available online at www.sciencedirect.com

ScienceDirect

ELSEVIER

Structural Insights into Immune Recognition of the Severe Acute Respiratory Syndrome Coronavirus S Protein Receptor Binding Domain

John E. Pak[1]†, **Chetna Sharon**[1,2]†, **Malathy Satkunarajah**[1,2], **Thierry C. Auperin**[1,2], **Cheryl M. Cameron**[3,4], **David J. Kelvin**[3,4], **Jayaraman Seetharaman**[5], **Alan Cochrane**[1], **Francis A. Plummer**[6], **Jody D. Berry**[6] and **James M. Rini**[1,2]*

[1]*Department of Molecular Genetics, University of Toronto, Toronto, Ontario, Canada M5S 1A8*

[2]*Department of Biochemistry, University of Toronto, Toronto, Ontario, Canada M5S 1A8*

[3]*University Health Network, Toronto, Ontario, Canada M5G 1L7*

[4]*University of Toronto, Toronto, Ontario, Canada M5S 1A8*

[5]*Brookhaven National Laboratory, Upton, NY 11973-5000, USA*

[6]*The National Microbiology Laboratory, Winnipeg, Manitoba, Canada R3E 3R2*

The spike (S) protein of the severe acute respiratory syndrome coronavirus (SARS-CoV) is responsible for host cell attachment and fusion of the viral and host cell membranes. Within S the receptor binding domain (RBD) mediates the interaction with angiotensin-converting enzyme 2 (ACE2), the SARS-CoV host cell receptor. Both S and the RBD are highly immunogenic and both have been found to elicit neutralizing antibodies. Reported here is the X-ray crystal structure of the RBD in complex with the Fab of a neutralizing mouse monoclonal antibody, F26G19, elicited by immunization with chemically inactivated SARS-CoV. The RBD–F26G19 Fab complex represents the first example of the structural characterization of an antibody elicited by an immune response to SARS-CoV or any fragment of it. The structure reveals that the RBD surface recognized by F26G19 overlaps significantly with the surface recognized by ACE2 and, as such, suggests that F26G19 likely neutralizes SARS-CoV by blocking the virus–host cell interaction.

*Corresponding author. E-mail address: james.rini@utoronto.ca.

† J.E.P. and C.S. contributed equally to this work.

Introduction

The etiological agent of severe acquired respiratory syndrome (SARS) is a recently identified coronavirus (SARS-CoV)[1–4] thought to have been transmitted to humans through contact with marketplace palm civets.[5] As with other members of the *Coronaviridae* family, SARS-CoV possesses a membrane glycoprotein called the spike (S) protein that mediates host cell attachment and fusion of the viral and host cell membranes. S is a type I transmem-

brane protein and can be described as having two functional regions: the N-terminal receptor binding region (S1) and the C-terminal membrane fusion region (S2).[6] The receptor for SARS-CoV is angiotensin-converting enzyme 2 (ACE2)[7] and the receptor binding domain (RBD, residues 318–510), located within S1, has been shown to be sufficient for ACE2 binding.[8,9] The X-ray crystal structure of the RBD–ACE2 complex has been determined and the structure shows that within the RBD, a large loop, called the receptor binding motif (RBM, residues 424–494), mediates all of the contacts with ACE2.[10] In addition, the structure provides insight into the role played by RBD residues thought to be important in the cross-species and human-to-human transmission of SARS-CoV.

The coronavirus S protein is also a major antigenic determinant and antibodies against S have been shown to be neutralizing for a number of coronaviruses.[11,12] In early work on SARS, mice immunized with chemically inactivated SARS-CoV were used to generate a panel of monoclonal antibodies capable of blocking infectivity in a cell-culture-based infectivity assay; of these, several were shown to be directed against the S protein.[13] Rabbit sera from animals vaccinated with an RBD-Fc fusion protein was shown to block binding of S1 to ACE2 and to neutralize SARS-CoV and SARS pseudovirus in a cell-based assay.[14] At the same time, immunization with the S protein was shown to provide protection against SARS-CoV in mice[15–17] and African green monkeys.[18] Given its role in receptor binding, the RBD was also tested as a vaccine candidate and found to provide protection in mice.[19,20] Although the rationalization for using the RBD is to elicit antibodies that would block receptor interactions, only a subset of the neutralizing antibodies raised against the RBD were found to directly compete with ACE2 binding.[21]

The screening of human antibody libraries derived from immune cells of individuals not exposed to SARS-CoV has also identified neutralizing antibody fragments that can prevent SARS-CoV infection.[22–24] Two of these antibody fragments (scFv 80R and Fab m396) have been characterized in complex with the RBD by X-ray crystallography,[22,25] and in both cases, the structures show that antibody binding would be expected to block the interaction with ACE2.

Reported here is the X-ray crystal structure of the Fab of a neutralizing mouse monoclonal antibody, F26G19, in complex with the RBD. F26G19 was elicited by immunization with chemically inactivated SARS-CoV and has been found to potently neutralize SARS-CoV (Tor2 strain) at 1 nM concentration in a cell-based assay.[13,26] The F26G19 Fab–RBD complex represents the first example of the structural characterization of an antibody elicited by an immune response to SARS-CoV or any fragment of it. The structure reveals that the RBD surface recognized by F26G19 overlaps significantly with the surface recognized by ACE2. As such, the structure suggests a mechanism of neutralization in

which antibody bound to the RBD blocks the binding of SARS-CoV to the host cell. Moreover, the complex provides further support for the continued development of the RBD as a SARS-CoV vaccine candidate.

Results

Overall structure of the F26G19 Fab–RBD complex

With the exception of the Fab elbow angles (169.9° and 186.0°), the two F26G19 Fab–RBD complexes in the asymmetric unit are found to be essentially identical. The two RBDs, the two variable light (V_L)/variable heavy (V_H) domains, and the two constant light (C_L)/constant heavy (C_H) domains superimpose with r.m.s.ds of 0.36, 0.40, and 0.49 Å, respectively. The nearly linear elbow angle is not uncommon for an IgG2a/kappa antibody,[27] and with the exception of the highly variable H3 complementarity determining region (CDR), the CDRs are found to adopt canonical conformations.[28] The 12-residue CDR H3 consists of two consecutive turns at approximate right angles to one another. ^{96}GIPQ^{99} compose the i to $i+3$ residues of a *cis*-proline type VIb turn that is found to interact extensively with RBD residue Ile489, while residues ^{99}QLLR^{100B} adopt a type I-like turn that predominately interacts with the Fab V_L domain.

Formation of the F26G19 Fab–RBD complex (Fig. 1) does not induce significant conformational changes in the RBD, as shown by a comparison with the free RBD[25] and the RBD–ACE2[10] complex. The RBD is composed of a five-stranded antiparallel β-sheet core and the RBM, the extended ACE2-binding loop that includes a small two-stranded antiparallel β-sheet and three short α-helices. As in the RBD–ACE2 complex, RBD residues 318–322 and 502–510 are disordered and are not observed in the electron density maps. The RBD contains three disulfide-bonded pairs of cysteine residues: Cys323/Cys348, Cys366/Cys419, and Cys467/Cys474. Notably, the RBD fragment used in determining the X-ray crystal structure of the Fab m396–RBD complex[22] was composed of residues 317–518 and that structure shows that Cys511, a residue not included in the 318–510 fragment used here, forms a disulfide bond with Cys378. The additional disulfide bond serves to immobilize the C-terminus of the RBD, resulting in the completion of a short three-stranded β-sheet, and electron density for residues 502–512 is observed in the Fab m396-RBD complex. The 318–510 fragment was also used in determining the structure of the free RBD; in that structure the RBD was found to form a dimer in the crystal lattice.[25] However, it should be noted that the native Cys378/Cys511 disulfide bond and the associated formation of the short three-stranded β-sheet is not structurally compatible with the observed dimer. We see no propensity for the 318–510 fragment to form dimers as determined by gel–filtration chromatography analysis at ∼10–100 μM concentration.
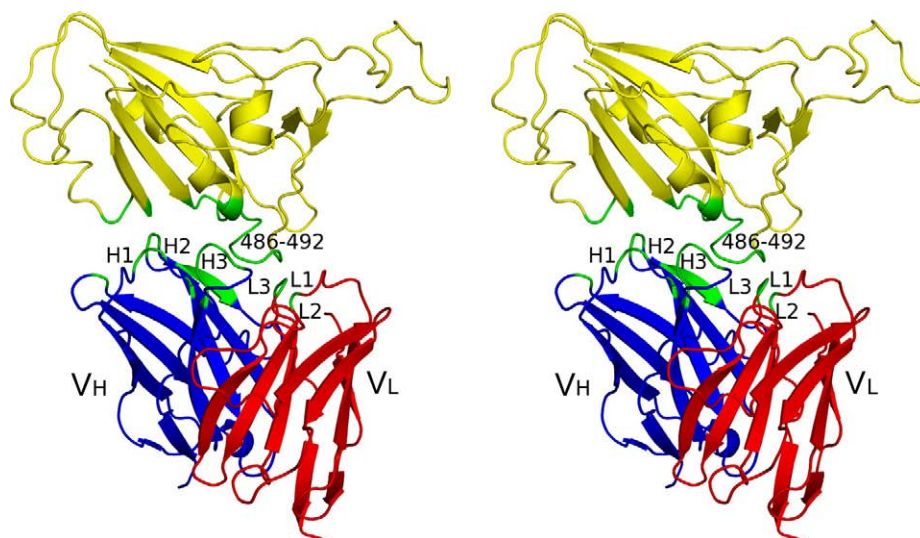
Fig. 1. Stereo ribbon representation of the F26G19 Fab–RBD binding interface. The RBD (in yellow) is shown in complex with the V_H (in blue) and V_L (in red) regions of the F26G19 Fab with the interface between the RBD and the Fab highlighted (in green). Residues 486–492 of the RBD are labeled and the CDRs of the Fab are labeled as H1, H2, H3, L1, L2, and L3. For simplicity, the C_L and C_H regions have been omitted from the figure.

The F26G19 Fab–RBD interface buries a total surface area of approximately 1400 Å^2 and is found to exhibit a high degree of electrostatic and shape complementarity[29] (S_c = 0.70). On the RBD, four discrete segments of polypeptide are buried in the interface. The four segments, residues 359–362, 391–392, 424–427, and 486–492, contribute 21%, 10%, 23%, and 46% to the total RBD surface buried, respectively. In addition, the buried RBD surface is flanked on one side by two N-linked glycosylation sites (Asn330 and Asn357). Both asparagine side chains point away from the RBD–Fab interface (see Fig. 3), and we have shown that carbohydrate does not interfere with binding; the affinity of the F26G19 Fab for the glycosylated (K_d = 2.6 × 10^{-8} M) and the deglycosylated RBD (K_d = 1.2 × 10^{-8} M) is very similar, as measured by BIAcore analysis (data not shown). Nearly all of the F26G19 Fab residues in the interface are contributed by the CDRs, with 76% of the surface area buried coming from the heavy-chain CDRs. The dominant role played by heavy-chain CDRs has also been observed in other Fab–antigen complexes.[30]

Determinants of F26G19 Fab binding

Although the F26G19 Fab recognizes a discontinuous epitope on the RBD, a linear segment, RBD residues 486–492 (46% of the RBD surface buried), is clearly the major determinant of binding. Structurally, residues 486–492 are part of a loop containing a type I β-turn that connects β-strands 6 and 7. This loop is well exposed in the structure of the free RBD[25] and in this Fab complex it is buried in the cleft formed by V_H and V_L. The 486–492 loop interacts primarily with CDR H3 (Glu95, Ile97, Asn99) and CDR L3 (Val92, Ser93, Tyr94), but additional interactions with CDR H1 (Arg33), CDR H2

(Tyr52), and CDR L1 (Tyr32) are also made (Fig. 2). The loop contacts with CDR L1 and CDR L3 represent the only interactions that the RBD makes with the V_L domain.

Of the residues in the 486–492 loop, Ile489 appears to be the most critical. It is the residue most deeply buried on complex formation (Fig. 2) and it is found near the centre of the interface. It sits in a pocket formed by the side chains of several V_H residues and Tyr494 of the RBD. On complex formation, 114 Å^2 of Ile489 is buried by CDR H1 Arg33, CDR H2 Tyr52, and CDR H3 Glu95/Ile97/Gln99. With the exception of this interaction, the only other side-chain interactions involving residues of the 486–492 loop are the weak hydrogen bonds that Tyr491 and Gln492 make with CDR L1 Tyr32 (3.1 Å) and CDR L3 Tyr94 (3.2 Å), respectively (Fig. 2). In contrast, hydrogen-bond interactions with the backbone of the loop appear to be much more important in complex formation. The backbone NH groups of loop residues 488–490 each donate hydrogen bonds to functional groups on the Fab (Fig. 2). In addition, the carbonyl oxygen of loop residue Thr486 accepts a hydrogen bond from the backbone NH of CDR L3 Tyr94. Also notable is loop residue Gly488, which along with Ile489 sits in a groove in the Fab that accommodates these two residues (Fig. 2). The C^α atom of Gly488 points into the surface of the Fab and mutation to any other residue type would be expected to disrupt the F26G19-RBD complex.

Structural basis of viral neutralization

As shown in Fig. 3, the 486–492 loop of the RBD forms a protrusion that separates the surfaces buried by ACE2 and the F26G19 Fab in their respective complexes. In fact, the overlap between these two surfaces is accounted for entirely by residues 486–
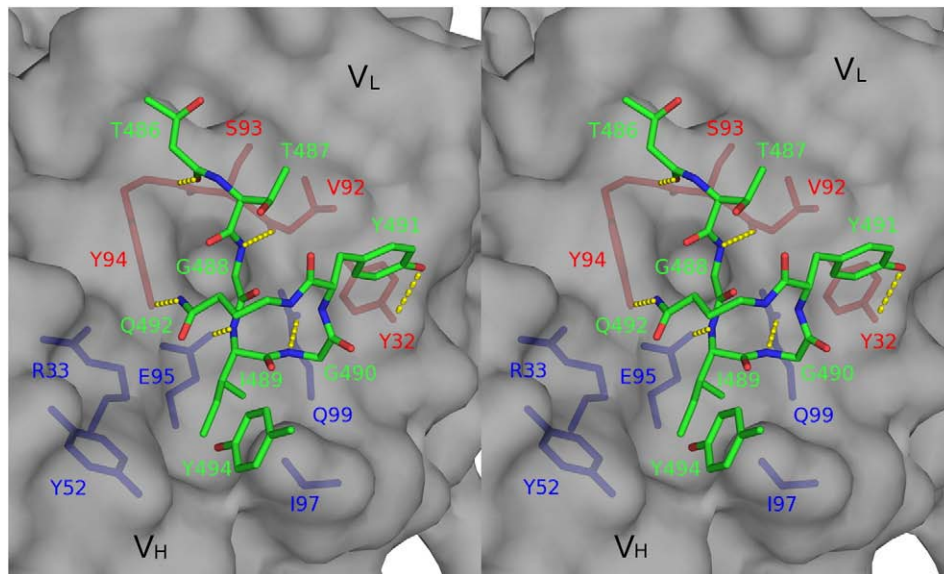
Fig. 2. Stereo diagram of the F26G19 Fab binding site for RBD residues 486–492. RBD residues 486–492 and 494 (green carbon atoms), as well as the F26G19 V_L (pink atoms) and V_H (blue atoms) residues that interact with the 486–492 loop are depicted in stick representation. The molecular surface of F26G19 Fab in the vicinity of the 486–492 loop is depicted (in grey). Intermolecular hydrogen bonds between RBD residues 486–492 and the F26G19 Fab are shown as yellow dashes.

491 and corresponds to 35% of the RBD surface buried by ACE2. In addition, nearly the entire volume of the V_L domain in the antibody complex occupies the same volume occupied by ACE2 in the RBD–ACE2 complex (Fig. 4). Thus, the ability of F26G19 to neutralize SARS-CoV infectivity likely stems from a direct competition between the antibody and ACE2 for binding to the RBD. Consistent with this suggestion is our BIAcore data, which show that the affinity of the F26G19 Fab for the RBD ($K_d = 2.6 \times 10^{-8}$ M) is comparable to the affinity of ACE2 for S1 ($K_d = 1.7 \times 10^{-9}$ M).[23] Two other neutralizing antibody fragments, Fab m396 and scFv 80R, which have been shown to compete with ACE2 for binding to the RBD,[22,23,25] have also been shown to bind with high affinity (2.0×10^{-8} M for the RBD and
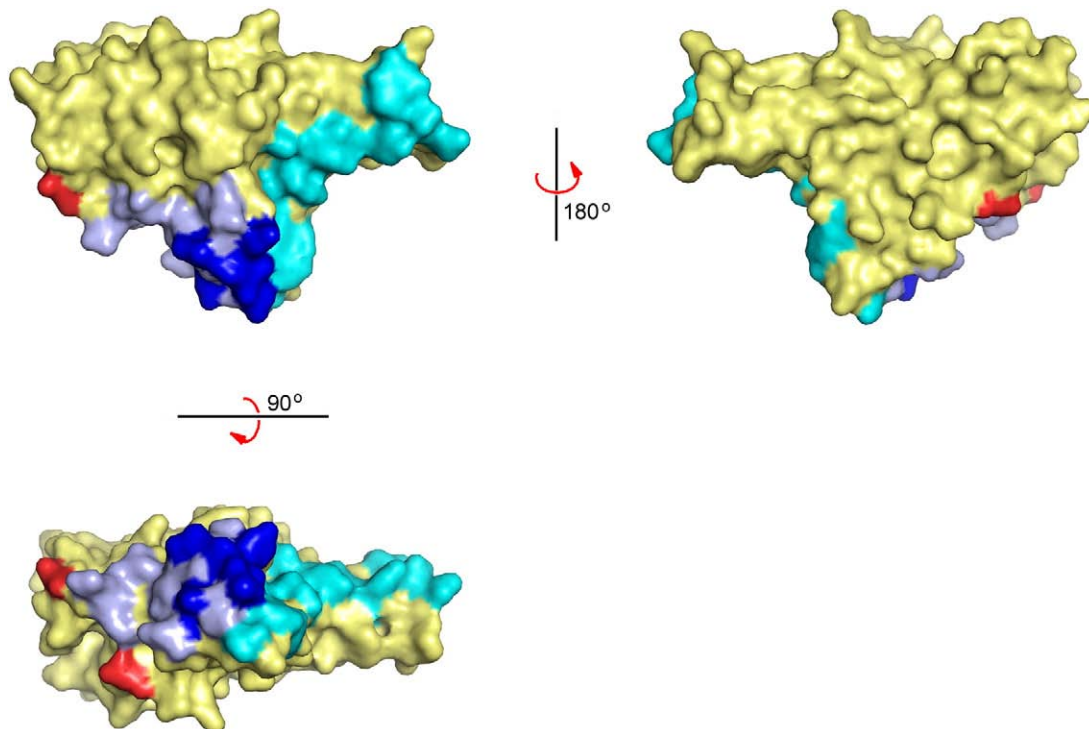

Fig. 3. Molecular surface representation of the F26G19 Fab and ACE2 binding sites on the RBD. The RBD surfaces buried by the F26G19 Fab (in light blue) and ACE2 (in turquoise) overlap at RBD residues 486–491 (in dark blue). The two N-linked glycosylation sites on the RBD (Asn330, Asn357) are illustrated (in red).
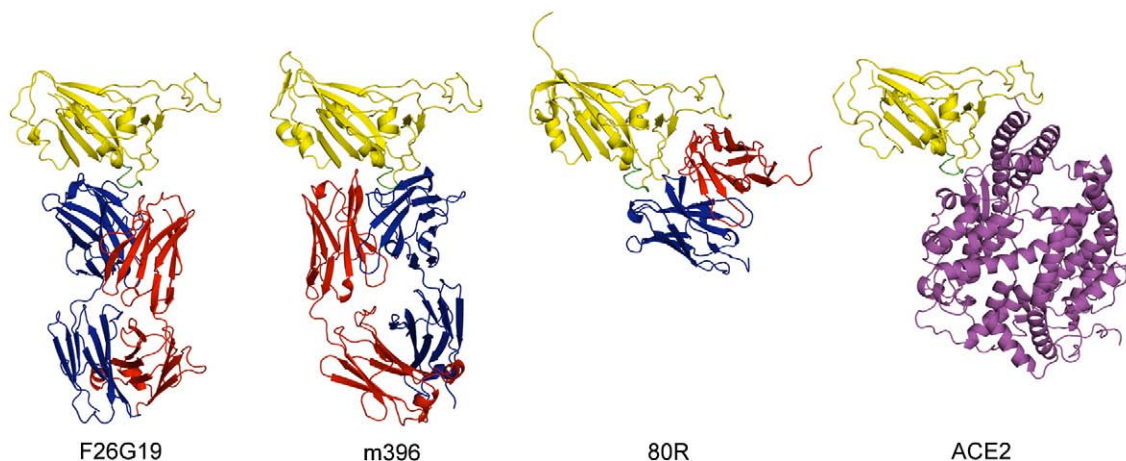
Fig. 4. Ribbon representation of the F26G19 Fab–RBD complex and the m396 Fab–RBD,[22] 80R scFv–RBD[25] and ACE2–RBD[10] complexes. The heavy chain and light chain of each neutralizing antibody fragment is depicted in blue and red, respectively, the RBD is depicted in yellow and the ACE2 molecule is depicted in purple. Residues 486–492 of the RBD, which represent the major determinant of F26G19 binding, are depicted in green.

3.2×10^{-8} M for S1, respectively). Remarkably, RBD residues 486–491 were also found to be a key determinant of recognition by Fab m396.[22] This antibody fragment, which exhibits a broad neutralizing activity for several different strains of SARS-CoV,[31] was selected from a naïve human library for its ability to bind to the RBD and was not elicited by an immune response to virus. In the Fab m396–RBD complex, the loop is even more extensively buried with 10 residues (482–491) constituting 51% of the total surface area buried by the antibody fragment. As shown in Fig. 4, the loop is also buried in the cleft formed between V_H and V_L in the Fab m396–RBD complex; however, the antibody fragment is rotated approximately 180° relative to that seen in the F26G19–RBD complex. Nevertheless, even though the relative positions of the heavy and light chains of the Fabs are "swapped" in the two complexes, the volumes occupied by the Fabs are very similar (Fig. 4). The nonimmune 80R antibody was also isolated from a human library derived from unimmunized donors and it exhibits potent neutralizing activity against the Tor2 and Urbani strains of SARS-CoV.[23,31] The X-ray crystal structure of the 80R scFv in complex with the RBD[25] shows that although the 486–492 loop is not buried as extensively as it is in the F26G19 and m396 complexes, the Fab overlaps even more fully with the volume occupied by ACE2 in the RBD–ACE2 complex (Fig. 4).

Discussion

F26G19 is a mouse monoclonal antibody elicited by immunization with chemically inactivated SARS-CoV. We have shown that the Fab of this antibody binds with high affinity to the SARS-CoV S protein RBD and we have determined the X-ray crystal structure of the Fab–RBD complex. The structure shows that while the RBD epitope recognized by F26G19 is discontinuous and conformational in

nature, a linear epitope (residues 486–492), formed by a surface-exposed loop on the RBD, is the major determinant of F26G19 binding. The loop is buried in the cleft formed between the heavy and light chains, with loop residue Ile489 making the most extensive contacts with the Fab. Interestingly, this loop is also found to be central to the interaction with the high-affinity neutralizing Fab m396 isolated from a naïve human antibody library,[22] suggesting that its conformation and/or surface exposure make it intrinsically well suited to antibody recognition and virus neutralization.

Antibody-mediated neutralization of enveloped viruses such as SARS-CoV is likely explained by a multihit model in which many, if not all, of the spike proteins on the virus surface are bound by antibody.[32–35] In fact, it has been proposed that the only requirement for neutralization is that the virus surface be coated with antibody so as to sterically prevent host cell attachment and/or membrane fusion.[32,34] It follows then that high-affinity antibodies such as F26G19, which compete directly for receptor binding, should be the most potent. Experimental support for this suggestion stems from a study of three influenza virus neutralizing antibodies, which showed that the two antibodies that bound the viral hemagglutinin and blocked sialic acid binding required a lower antibody–hemagglutinin ratio to block the virus–host cell interaction.[36,37] Like F26G19, the antibody fragments m396 and 80R also compete with ACE2 for binding to the RBD.[22,23,25] This, coupled with the fact that they both bind the RBD with high affinity although they are from antibody libraries derived from unimmunized donors, presumably explains their ability to potently neutralize infectivity.[22,25] The observation that some SARS-CoV-neutralizing antibodies do not compete with ACE2 for RBD binding[21,38] nevertheless shows that direct competition is not necessarily required for antibody-mediated neutralization of SARS-CoV.

Given that SARS-CoV binds the large (723 amino acids) globular domain of membrane-bound ACE2, it follows that the RBD is either relatively exposed on the viral surface or that it becomes exposed during the process of host cell binding. Support for the former is provided for by single-particle cryoelectron microscopy reconstructions of SARS-CoV[39] and the SARS-CoV–ACE2 complex,[40] which show that the S1 region of the trimeric S protein is exposed like the blades of a propeller and that each monomer of the trimer binds to an ACE2 molecule. Since F26G19 and ACE2 occupy overlapping volumes when bound to the RBD (Fig. 4), it follows that antibodies such as F26G19 would be equally well accommodated by each monomer of the native trimer found on the viral membrane. Since these reconstructions also show that the ACE2 molecules point away from the viral membrane along the long axis of the trimer, antibodies bound to the RBD would be well disposed to sterically block interactions with the cell surface. Further support for the suggestion that the RBD is readily accessible on the viral surface stems from the fact that the neutralizing antibodies m396 and 80R are also presumably accommodated, although the way they interact with the RBD would place the Fc domain and the "other" Fab arm of the immunoglobulin in locations different from that of F26G19. The presumed exposure of the SARS RBD and its high affinity for the large ACE2 receptor have been the subject of previous discussion and it has been suggested that this may reflect a virus that has yet to evolve to evade the immune system or one that favors rapid transmission over immune escape.[5,41] Consistent with this suggestion is the critical role played by Ile89 in F26G19 binding. This surface-exposed residue is not involved in ACE2 binding and its mutation would presumably lead to escape from F26G19-like antibodies. The exposure of the RBD may also explain why the monomeric RBD is a good vaccine candidate even though the S protein is trimeric.[19] Owing to the separation of the RBDs in the native trimer, antibody interactions presumably involve only one subunit (as with the ACE2 interaction) and, as such, the monomeric RBD would conceivably elicit the same neutralizing antibodies that it would in the context of the trimer. This property is to be contrasted with that seen for both the influenza virus hemagglutinin and HIV gp120/41, where the trimeric state of the viral fusion protein is critical for eliciting a good neutralizing antibody response.[42,43]

Carbohydrate is another means by which viruses limit the exposure of their RBDs to protect themselves from eliciting receptor-blocking antibodies, although it seems that this strategy is not employed by SARS-CoV. The SARS-CoV S protein possesses 23 N-linked oligosaccharide sites, 3 of which are in the RBD, and analysis shows that those in the RBD are clustered toward one end of the domain distant from the ACE2 binding site (see Fig. 3). As such, these carbohydrates would not be expected to affect ACE2 binding. Indeed, our BIAcore measurements show that F26G19 binds the glycosylated and the deglycosylated RBD with essentially the same affinity. The fact that the RBD does not possess carbohydrate in the immediate vicinity of the ACE2 binding site is in contrast with that found in other viruses. In the case of HIV gp120/41, for example, carbohydrate is found to ring the CD4 binding site,[42,44] thereby greatly reducing the likelihood of eliciting an antibody whose footprint partially overlaps with that of the receptor binding surface. Only 46% of the F26G19 footprint on the RBD overlaps with that of the ACE2 footprint and, as such, there is RBD surface area (54%) available for the acquisition of N-linked oligosaccharides that would block F26G19 antibody binding but not ACE2 binding. The fact that there is more than one type of neutralizing antibody (i.e., antibodies that do not compete with each other for RBD binding) that can compete with ACE2 binding[21,38] further suggests that multiple regions adjacent to the ACE2 binding site are accessible for antibody binding. The F26G19 Fab covers only 35% of the RBD surface buried by ACE2, and partial overlap would presumably be sufficient for other neutralizing antibodies that compete directly with ACE2 binding. That carbohydrate does not ring the ACE2 binding site on the RBD may well support the suggestion that the observed RBD–ACE2 interaction, mediated as it is through the RBM, is a recent acquisition.[5,45] Nevertheless, it should be noted that the presence of carbohydrate on the RBD is not without consequence. The fully glycosylated RBD gives a higher neutralizing antibody titre than that of the deglycosylated form, an effect attributed to a reduction in antibodies directed against nonneutralizing epitopes.[19]

Based on the fact that all of the ACE2 interactions with the RBD are entirely mediated through the RBM, it has been suggested that the RBM might serve as a good SARS-CoV vaccine candidate.[10] Indeed, loop residues 486–492, which are part of the RBM, form a protrusion on the RBD that is central to the interaction with F26G19 and the naïve antibody fragment Fab m396. In both cases, however, interactions with residues not included in the RBM are important, and the RBM alone might not elicit high-affinity F26G19-like antibodies. Moreover, given that the RBD has also been shown to be capable of generating several different classes of neutralizing antibodies—both competitive and noncompetitive with ACE2 binding[21,38]—it seems clear that the RBD holds considerable promise as a robust SARS-CoV vaccine candidate.

Materials and Methods

Expression and purification of the SARS-CoV RBD

A stably transformed HEK-293T cell line secreting a protein A–RBD fusion protein was generated using protocols previously described.[46] Briefly, a codon-optimized fragment of the RBD (residues 318–510) was subcloned into pPA-TEV, an expression vector supplying the transin leader sequence, an N-terminal protein A fusion tag, and

the TEV protease recognition sequence. The resulting pPA-TEV-RBD vector was linearized and HEK-293T cells grown in Iscove's modified Dulbecco's medium supplemented with 10% fetal bovine serum and 1 mg/l aprotinin were transfected using the calcium phosphate method. Stably transformed cell lines were selected and cloned using 1 μg/ml puromycin. Protein production was scaled up in a Celligen 2.2-l New Brunswick bioreactor using the basket impeller containing 30 g of FibraCel disks (New Brunswick, M11769984). Once the culture was established, CHO-S-SFM-II medium supplemented with 3% fetal bovine serum, 2.25 g/l glucose, 1× nonessential amino acids, 1 mg/l aprotinin, and 1× penicillin–streptomycin was supplied in perfusion mode at ~3–4 l/day for 15 days. The harvested medium was concentrated 10-fold and the protein A–RBD fusion protein was purified by IgG Sepharose affinity chromatography. The fusion protein was eluted with 0.1 M glycine (pH 3.0) and the protein A tag was removed by overnight TEV protease digestion at 4 °C using a TEV–protein A-RBD ratio of 1:6 (w/w). The RBD was further purified by phenyl-Sepharose hydrophobic interaction and Q-Sepharose ion-exchange chromatography. N-linked oligosaccharides were removed by overnight peptide–N-glycosidase F (PNGase F) digestion at a PNGase F–RBD ratio of 3:1(w/w) in 10 mM Tris (pH 8), 7% glycerol, 120 mM NaCl, and 1 mM ethylenediaminetetraacetic acid (EDTA) at 37 °C. The deglycosylated RBD was further purified by Q-Sepharose ion-exchange and Superdex 200 gel-filtration chromatography (GE Healthcare) and concentrated to 0.2 mg/ml in 20 mM sodium acetate buffer (pH 5) containing 150 mM NaCl and 1 mM EDTA. Both the glycosylated and the PNGase F-treated RBD existed solely as monomers when analyzed by gel-filtration chromatography at concentrations between ~10 and 100 μM.

Production and purification of the F26G19 Fab

Murine monoclonal antibody F26G19[13,26] [accession numbers AY605279 (V_L) and AY605270 (V_H)], whose V_H gene is most similar to the human V_H gene allele *IGHV1-f*01*, was incubated with papain at an antibody–enzyme ratio of 100:1 (w/w) in phosphate-buffered saline (pH 7) containing 2 mM cysteine and 0.4 mM EDTA for 8 h at 37 °C. Papain digestion was stopped by incubation with 100 mM iodoacetamide for 30 min at room temperature. The Fab was then dialyzed against 10 mM Tris buffer (pH 8) and purified by mono Q-Sepharose ion-exchange chromatography followed by dialysis and concentration to 0.5 mg/ml in 20 mM sodium acetate buffer (pH 5) containing 150 mM NaCl and 1 mM EDTA.

Surface plasmon resonance affinity measurements

Real-time surface plasmon resonance measurements were performed on a BIAcore X instrument. CM5 sensor chips were immobilized with either F26G19 Fab or deglycosylated RBD using solutions containing protein at a concentration of 25–50 μg/ml in 10 mM sodium acetate buffer (pH 5–5.5). A reference surface, created via mock immobilization with 10 mM sodium acetate buffer (pH 5–5.5) was used to correct for nonspecific binding and bulk refractive index changes. The analytes, Fab or RBD as appropriate, were dialyzed against HBS-EP [10 mM Hepes (pH 7.5), 150 mM NaCl, 3 mM EDTA, 0.005% Surfactant P20] and injected for 140 s at a flow rate of 30 μl/min at 25 °C. Sensor chips were regenerated with a 20-s pulse of a 1/200 dilution of phosphoric acid. All data were fit to a 1:1 binding isotherm using the BIAevaluation software.

F26G19 Fab–RBD complex crystallization and data collection

RBD and F26G19 Fab were mixed at a molar ratio of 1.4:1 and concentrated to 6 mg/ml. The F26G19 Fab–RBD complex was then purified by Superdex 200 gel-filtration chromatography in 20 mM sodium acetate buffer (pH 5) containing 150 mM NaCl and 1 mM EDTA and concentrated to 4.5 mg/ml. Crystals of the RBD–F26G19 Fab complex grew in 2–3 days using the hanging-drop vapor-diffusion method with 1 μl of the F26G19 Fab–RBD solution and 1 μl of well solution [0.1 M Mes (pH 5.5), 14% PEG (polyethylene glycol) 20000, and 10–15% glycerol]. A 3.0 Å data set was collected on beam line X12C at the National Synchrotron Light Source (NSLS) from crystals frozen in 0.1 M Mes (pH 5.5), 14% PEG 20000, and 30% glycerol. Data were processed using HKL2000[47] as summarized in Table 1.

Structure determination and refinement

The structure of the F26G19 Fab–RBD complex was solved by molecular replacement using the program PHASER.[48] A series of Fab molecules varying in elbow angle were used as molecular replacement search models. A Fab with an elbow angle close to 180° [Protein Data Bank (PDB) code IKEG] was found to give the cleanest rotation function solution. The hypervariable loops of 1KEG were

Table 1. Crystallographic statistics

Data collection	
Source	NSLS X12C
Space group	$P2_12_12$
Cell dimensions	
a, b, c (Å)	183.69, 73.36, 110.78
α, β, γ (°)	90, 90, 90
Resolution	50–2.8
Wavelength (Å)	0.979
Unique reflections	35,508
Redundancy	5.2 (4.4)[a]
Completeness (%)	94.4 (92.5)
R_{merge} (%)	13.2 (51.0)
$I/\sigma(I)$	11.9 (2.7)
Refinement	
Resolution	30–3.0
R_{work} (%)	23.5
R_{free} (%)	28.6
No. of molecules	
Protein	9414
Water	6
B-factors	
Protein	47.4
Water	25.5
r.m.s.d.	
Bond lengths (Å)	0.006
Bond angles (°)	1.1
Ramachandran plot	
Most favored (%)	84.6
Additionally allowed (%)	14.6
Generously allowed (%)	0.6
Disallowed (%)	0.2

[a] Values in parentheses correspond to statistics for the (3.15–3.02 Å) resolution shell.

then removed and this Fab molecule, along with the RBD structure (PDB code 2DDB), was then used to solve the structure. Two F26G19 Fab–RBD complexes were found in the asymmetric unit. Rigid-body refinement and simulating annealing were performed using CNS 1.1,[49] and restrained positional refinement, *B*-factor refinement, and TLS parameterization were performed using REFMAC.[50] Model building was performed with the program Coot.[51] The structure was refined to 3.0 Å; the model building and refinement statistics are summarized in Table 1.

PDB accession number

The atomic coordinates and structure factors have been deposited in the PDB with accession number 3BGF.

References

1. Drosten, C., Gunther, S., Preiser, W., van der Werf, S., Brodt, H. R., Becker, S. *et al.* (2003). Identification of a novel coronavirus in patients with severe acute respiratory syndrome. *N. Engl. J. Med.* **348**, 1967–1976.
2. Ksiazek, T. G., Erdman, D., Goldsmith, C. S., Zaki, S. R., Peret, T., Emery, S. *et al.* (2003). A novel coronavirus associated with severe acute respiratory syndrome. *N. Engl. J. Med.* **348**, 1953–1966.
3. Peiris, J. S., Lai, S. T., Poon, L. L., Guan, Y., Yam, L. Y., Lim, W. *et al.* (2003). Coronavirus as a possible cause of severe acute respiratory syndrome. *Lancet*, **361**, 1319–1325.
4. Rota, P. A., Oberste, M. S., Monroe, S. S., Nix, W. A., Campagnoli, R., Icenogle, J. P. *et al.* (2003). Characterization of a novel coronavirus associated with severe acute respiratory syndrome. *Science*, **300**, 1394–1399.
5. Li, W., Wong, S. K., Li, F., Kuhn, J. H., Huang, I. C., Choe, H. & Farzan, M. (2006). Animal origins of the severe acute respiratory syndrome coronavirus: insight from ACE2–S-protein interactions. *J. Virol.* **80**, 4211–4219.
6. Gallagher, T. M. & Buchmeier, M. J. (2001). Coronavirus spike proteins in viral entry and pathogenesis. *Virology*, **279**, 371–374.
7. Li, W., Moore, M. J., Vasilieva, N., Sui, J., Wong, S. K., Berne, M. A. *et al.* (2003). Angiotensin-converting enzyme 2 is a functional receptor for the SARS coronavirus. *Nature*, **426**, 450–454.
8. Xiao, X., Chakraborti, S., Dimitrov, A. S., Gramatikoff, K. & Dimitrov, D. S. (2003). The SARS-CoV S glycoprotein: expression and functional characterization. *Biochem. Biophys. Res. Commun.* **312**, 1159–1164.
9. Wong, S. K., Li, W., Moore, M. J., Choe, H. & Farzan, M. (2004). A 193-amino acid fragment of the SARS coronavirus S protein efficiently binds angiotensin-converting enzyme 2. *J. Biol. Chem.* **279**, 3197–3201.
10. Li, F., Li, W., Farzan, M. & Harrison, S. C. (2005). Structure of SARS coronavirus spike receptor-binding domain complexed with receptor. *Science*, **309**, 1864–1868.
11. Saif, L. J. (1993). Coronavirus immunogens. *Vet. Microbiol.* **37**, 285–297.
12. Cavanagh, D. (1995). The coronavirus surface glycoprotein. In *The Coronaviridae* (Siddell, S., ed.), pp. 73–114, Plenum Press, New York.
13. Berry, J. D., Jones, S., Drebot, M. A., Andonov, A., Sabara, M., Yuan, X. Y. *et al.* (2004). Development and characterisation of neutralising monoclonal antibody to the SARS-coronavirus. *J. Virol. Methods*, **120**, 87–96.
14. He, Y., Zhou, Y., Liu, S., Kou, Z., Li, W., Farzan, M. & Jiang, S. (2004). Receptor-binding domain of SARS-CoV spike protein induces highly potent neutralizing antibodies: implication for developing subunit vaccine. *Biochem. Biophys. Res. Commun.* **324**, 773–781.
15. Bisht, H., Roberts, A., Vogel, L., Bukreyev, A., Collins, P. L., Murphy, B. R. *et al.* (2004). Severe acute respiratory syndrome coronavirus spike protein expressed by attenuated vaccinia virus protectively immunizes mice. *Proc. Natl Acad. Sci. USA*, **101**, 6641–6646.
16. Yang, Z. Y., Kong, W. P., Huang, Y., Roberts, A., Murphy, B. R., Subbarao, K. & Nabel, G. J. (2004). A DNA vaccine induces SARS coronavirus neutralization and protective immunity in mice. *Nature*, **428**, 561–564.
17. See, R. H., Zakhartchouk, A. N., Petric, M., Lawrence, D. J., Mok, C. P., Hogan, R. J. *et al.* (2006). Comparative evaluation of two severe acute respiratory syndrome (SARS) vaccine candidates in mice challenged with SARS coronavirus. *J. Gen. Virol.* **87**, 641–650.
18. Bukreyev, A., Lamirande, E. W., Buchholz, U. J., Vogel, L. N., Elkins, W. R., St Claire, M. *et al.* (2004). Mucosal immunisation of African green monkeys (*Cercopithecus aethiops*) with an attenuated parainfluenza virus expressing the SARS coronavirus spike protein for the prevention of SARS. *Lancet*, **363**, 2122–2127.
19. Zakhartchouk, A. N., Sharon, C., Satkunarajah, M., Auperin, T., Viswanathan, S., Mutwiri, G. *et al.* (2007). Immunogenicity of a receptor-binding domain of SARS coronavirus spike protein in mice: implications for a subunit vaccine. *Vaccine*, **25**, 136–143.
20. Du, L., Zhao, G., He, Y., Guo, Y., Zheng, B. J., Jiang, S. & Zhou, Y. (2007). Receptor-binding domain of SARS-CoV spike protein induces long-term protective immunity in an animal model. *Vaccine*, **25**, 2832–2838.
21. He, Y., Lu, H., Siddiqui, P., Zhou, Y. & Jiang, S. (2005). Receptor-binding domain of severe acute respiratory syndrome coronavirus spike protein contains multiple conformation-dependent epitopes that induce highly potent neutralizing antibodies. *J. Immunol.* **174**, 4908–4915.
22. Prabakaran, P., Gan, J., Feng, Y., Zhu, Z., Choudhry, V., Xiao, X. *et al.* (2006). Structure of severe acute respiratory syndrome coronavirus receptor-binding domain complexed with neutralizing antibody. *J. Biol. Chem.* **281**, 15829–15836.
23. Sui, J., Li, W., Murakami, A., Tamin, A., Matthews, L. J., Wong, S. K. *et al.* (2004). Potent neutralization of severe acute respiratory syndrome (SARS) coronavirus by a human mAb to S1 protein that blocks

receptor association. *Proc. Natl Acad. Sci. USA*, **101**, 2536–2541.

24. van den Brink, E. N., Ter Meulen, J., Cox, F., Jongeneelen, M. A., Thijsse, A., Throsby, M. *et al.* (2005). Molecular and biological characterization of human monoclonal antibodies binding to the spike and nucleocapsid proteins of severe acute respiratory syndrome coronavirus. *J. Virol.* **79**, 1635–1644.

25. Hwang, W. C., Lin, Y., Santelli, E., Sui, J., Jaroszewski, L., Stec, B. *et al.* (2006). Structural basis of neutralization by a human anti-severe acute respiratory syndrome spike protein antibody, 80R. *J. Biol. Chem.* **281**, 34610–34616.

26. Gubbins, M. J., Plummer, F. A., Yuan, X. Y., Johnstone, D., Drebot, M., Andonova, M. *et al.* (2005). Molecular characterization of a panel of murine monoclonal antibodies specific for the SARS-coronavirus. *Mol. Immunol.* **42**, 125–136.

27. Stanfield, R. L., Zemla, A., Wilson, I. A. & Rupp, B. (2006). Antibody elbow angles are influenced by their light chain class. *J. Mol. Biol.* **357**, 1566–1574.

28. Al-Lazikani, B., Lesk, A. M. & Chothia, C. (1997). Standard conformations for the canonical structures of immunoglobulins. *J. Mol. Biol.* **273**, 927–948.

29. Lawrence, M. C. & Colman, P. M. (1993). Shape complementarity at protein/protein interfaces. *J. Mol. Biol.* **234**, 946–950.

30. Wilson, I. A. & Stanfield, R. L. (1994). Antibody–antigen interactions: new structures and new conformational changes. *Curr. Opin. Struct. Biol.* **4**, 857–867.

31. Zhu, Z., Chakraborti, S., He, Y., Roberts, A., Sheahan, T., Xiao, X. *et al.* (2007). Potent cross-reactive neutralization of SARS coronavirus isolates by human monoclonal antibodies. *Proc. Natl Acad. Sci. USA*, **104**, 12123–12128.

32. Burton, D. R., Williamson, R. A. & Parren, P. W. (2000). Antibody and virus: binding and neutralization. *Virology*, **270**, 1–3.

33. Klasse, P. J. & Sattentau, Q. J. (2002). Occupancy and mechanism in antibody-mediated neutralization of animal viruses. *J. Gen. Virol.* **83**, 2091–2108.

34. Parren, P. W. & Burton, D. R. (2001). The antiviral activity of antibodies in vitro and in vivo. *Adv. Immunol.* **77**, 195–262.

35. Reading, S. A. & Dimmock, N. J. (2007). Neutralization of animal virus infectivity by antibody. *Arch. Virol.* **152**, 1047–1059.

36. Knossow, M., Gaudier, M., Douglas, A., Barrere, B., Bizebard, T., Barbey, C. *et al.* (2002). Mechanism of neutralization of influenza virus infectivity by antibodies. *Virology*, **302**, 294–298.

37. Knossow, M. & Skehel, J. J. (2006). Variation and infectivity neutralization in influenza. *Immunology*, **119**, 1–7.

38. He, Y., Li, J., Li, W., Lustigman, S., Farzan, M. & Jiang, S. (2006). Cross-neutralization of human and palm civet severe acute respiratory syndrome corona-viruses by antibodies targeting the receptor-binding domain of spike protein. *J. Immunol.* **176**, 6085–6092.

39. Beniac, D. R., Andonov, A., Grudeski, E. & Booth, T. F. (2006). Architecture of the SARS coronavirus prefusion spike. *Nat. Struct. Mol. Biol.* **13**, 751–752.

40. Beniac, D. R., Devarennes, S. L., Andonov, A., He, R. & Booth, T. F. (2007). Conformational reorganization of the SARS coronavirus spike following receptor binding: implications for membrane fusion. *PLoS ONE*, **2**, e1082.

41. Yang, Z. Y., Werner, H. C., Kong, W. P., Leung, K., Traggiai, E., Lanzavecchia, A. & Nabel, G. J. (2005). Evasion of antibody neutralization in emerging severe acute respiratory syndrome coronaviruses. *Proc. Natl Acad. Sci. USA*, **102**, 797–801.

42. Pantophlet, R. & Burton, D. R. (2006). GP120: target for neutralizing HIV-1 antibodies. *Annu. Rev. Immunol.* **24**, 739–769.

43. Wei, C. J., Xu, L., Kong, W. P., Shi, W., Canis, K., Stevens, J. *et al.* (2008). Comparative efficacy of neutralizing antibodies elicited by recombinant hemagglutinin proteins from avian H5N1 influenza virus. *J. Virol.* **82**, 6200–6208.

44. Koch, M., Pancera, M., Kwong, P. D., Kolchinsky, P., Grundner, C., Wang, L. *et al.* (2003). Structure-based, targeted deglycosylation of HIV-1 gp120 and effects on neutralization sensitivity and antibody recognition. *Virology*, **313**, 387–400.

45. Li, W., Zhang, C., Sui, J., Kuhn, J. H., Moore, M. J., Luo, S. *et al.* (2005). Receptor and viral determinants of SARS-coronavirus adaptation to human ACE2. *EMBO J.* **24**, 1634–1643.

46. Pak, J. E. & Rini, J. M. (2006). X-ray crystal structure determination of mammalian glycosyltransferases. *Methods Enzymol.* **416**, 30–48.

47. Otwinowski, Z. & Minor, W. (1997). Processing of X-ray diffraction data collected in oscillation mode. In *Methods in Enzymology* (Carter, C. W., Jr, ed.), 276, pp. 307–326Academic Press, Orlando, FL.

48. McCoy, A. J., Grosse-Kunstleve, R. W., Storoni, L. C. & Read, R. J. (2005). Likelihood-enhanced fast translation functions. *Acta Crystallogr., Sect. D: Biol. Crystallogr.* **61**, 458–464.

49. Brunger, A. T., Adams, P. D., Clore, G. M., DeLano, W. L., Gros, P., Grosse-Kunstleve, R. W. *et al.* (1998). Crystallography & NMR system: a new software suite for macromolecular structure determination. *Acta Crystallogr., Sect D: Biol. Crystallogr.* **54**, 905–921.

50. Murshudov, G. N., Vagin, A. A. & Dodson, E. J. (1997). Refinement of macromolecular structures by the maximum-likelihood method. *Acta Crystallogr., Sect. D: Biol. Crystallogr.* **53**, 240–255.

51. Emsley, P. & Cowtan, K. (2004). Coot: model-building tools for molecular graphics. *Acta Crystallogr., Sect. D: Biol. Crystallogr.* **60**, 2126–2132.